

A FRAMEWORK FOR POSITION UNCERTAINTY OF UNORGANISED THREE-DIMENSIONAL POINT CLOUDS FROM NEAR-MONOSTATIC LASER SCANNERS USING COVARIANCE ANALYSIS

Kwang-Ho Bae¹, David Belton^{1,2}, and Derek D. Lichti^{1,2}

Department of Spatial Sciences, Curtin University of Technology, Perth, WA, 6845, Australia¹

Cooperative Research Centre for Spatial Information, Australia²

baek@vesta.curtin.edu.au, beltondm@vesta.curtin.edu.au, d.lichti@curtin.edu.au

KEY WORDS: Position uncertainty, Three-dimensional, Point Cloud, Laser Scanning

ABSTRACT

Position uncertainty is one of the most important quantities of an unorganised three-dimensional point clouds since it provides the confidence level of any parametric estimation such as surface normal vector estimation and the registration of point clouds. We present an explicit form of position uncertainty based on the covariance analysis of a point. In addition, an explicit form of the variance of an estimated surface normal vector and an algorithm to evaluate an optimal size of the neighbourhood of a point which minimises the variance of the estimated normal vector are presented.

1 INTRODUCTION

Position uncertainty of a point in an unorganised point cloud measured by a range sensor is one of the most important quantities since it provides the confidence level of any parametric estimation such as surface normal vector estimation and the registration of point clouds (Bae and Lichti, 2004). However, in practice, to evaluate the position uncertainty from data is very difficult and more so is its derivation in explicit form, mainly because position uncertainty depends on the design of a measurement system, i.e. a laser and a detector in a laser scanner. One of the important factors in position uncertainty is the incidence angle of laser beam to the surface of scanned objects. The incidence angles of the laser beam from two different laser scanner locations are shown in Figure 1. The incidence angle of the laser beam is defined as the angle between the estimated surface normal vector and the line of sight of the laser beam. In addition, Figure 1 shows that there is about 40° of incidence angle difference in the overlapping regions, i.e. the common regions, of the point clouds. This large difference of incidence angles implies that position uncertainties of those regions are quite different. This implies that large error in either the estimation of surface normal vector or the registration of point clouds is expected without the consideration of position uncertainty of measurement by laser scanners.

Tasdizen and Whitaker (2003) found an explicit form of the Cramer-Rao lower bound of measurements by a range sensor with the assumption that the variance of the estimated geometric surface normal vector is small. Note that there are some minor errors in their derivation so the final result is not correct. Since the variance of estimated surface normal vectors is approximately proportional to that of the incidence angle, it can not be ignored although it is expected to be relatively small in the cases of close-range and terrestrial laser scanners. However, we need to quantify how relatively small it is to compare with the case in which this effect is ignored. In this paper, we correct Tasdizen and Whitaker (2003)'s results and present a more

precise form of the Cramer-Rao lower bound of measurements by a range sensor by including the variance of the estimated surface normal vector.

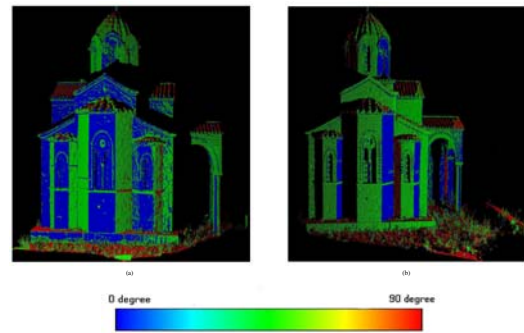


Figure 1: Color maps of incident angles of the Agia Samarina church in Greece scanned from two different locations using a Leica HDS2500. The radial and angular variances of the scanner are $\sigma_r^2 = (0.004)^2$ (m²) and $\sigma_a^2 = (6 \times 10^{-5})^2$ (rad²), respectively. The numbers of points for (a) and (b) are 486340 and 453142, respectively. The radial distance between the church and the scanner is approximately 20m in both cases. The dimension of the church is approximately $(L, W, H) = (25.0\text{m}, 15.0\text{m}, 10.0\text{m})$ where L , W , and H are the length, width, and height, respectively, of the object.

2 UVZ COORDINATE SYSTEM

Let us introduce four coordinate systems: the scanner coordinate system ($\mathbf{O}_{scanner}$), the laser beam coordinate system (\mathbf{O}_{laser}), the measured point coordinate system (\mathbf{O}_{point}) and the uvz coordinate system (\mathbf{O}_{uvz}) as shown in Figure 2. A laser scanner measures the radial distance in \mathbf{O}_{laser} in fixed horizontal and vertical angular intervals, i.e. two angular components of a spherical coordinate system. The measured position recorded in the spherical coordinate is transformed to a Cartesian coordinate system, i.e. $\mathbf{O}_{scanner}$.

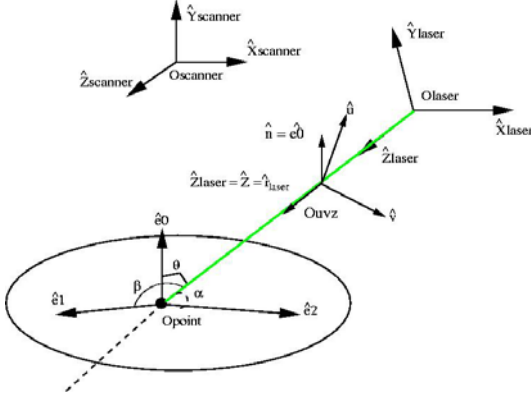


Figure 2: \hat{e}_i is the eigenvector of the i th largest eigenvalue of the covariance matrix (Bae and Lichti, 2004). θ , α , and β are the direction cosine angles of \hat{z}_{laser} relative to the local surface of an object in a scene. Note that $\hat{r}_{laser} = \hat{z} = \hat{z}_{laser}$ where \hat{r}_{laser} is a radial distance in \mathbf{O}_{laser} .

In this section we introduce a Cartesian coordinate system which is constructed by the surface normal vector and \hat{z}_{laser} , the line of sight of a scanner, as shown in Fig. 2. This coordinate system is important since it acts like a bridge between \mathbf{O}_{laser} and \mathbf{O}_{point} . Any vector or matrix in \mathbf{O}_{laser} can be approximately expressed in the uvz coordinate system without the knowledge of the rotation between them. Especially if the components of a matrix in the direction of \hat{x}_{laser} and \hat{y}_{laser} are the same, then so are they in the uvz coordinate system as shown in Eqs. 2. Note that $\mathbf{A} \times \mathbf{B}$ and (\mathbf{A}, \mathbf{B}) are the cross and dot products between vectors \mathbf{A} and \mathbf{B} , respectively. In addition, a vector in this paper is a column matrix. Let \hat{z}_{laser} and \hat{e}_0 be \hat{z} and \hat{n} , respectively. Then the unit vectors of the uvz coordinate system are expressed as follows

$$\begin{aligned}\hat{u} &= \hat{z} \times \hat{v} \\ \hat{v} &= \hat{n} \times \hat{z}\end{aligned}\quad (1)$$

and

$$\begin{aligned}\hat{x}_{laser} \times \hat{v} &= -\hat{z}(\hat{x}_{laser}, \hat{n}) \\ \hat{y}_{laser} \times \hat{v} &= -\hat{z}(\hat{y}_{laser}, \hat{n}) \\ \hat{x}_{laser} \times \hat{u} &= \hat{z}(\hat{x}_{laser}, \hat{v}) \\ \hat{y}_{laser} \times \hat{u} &= \hat{z}(\hat{y}_{laser}, \hat{v})\end{aligned}\quad (2)$$

using $\mathbf{A} \times (\mathbf{B} \times \mathbf{C}) = \mathbf{B}(\mathbf{A}, \mathbf{C}) - \mathbf{C}(\mathbf{A}, \mathbf{B})$ with vectors \mathbf{A} , \mathbf{B} , and \mathbf{C} . This shows that two planes whose tangential vectors are $\{\hat{u}, \hat{v}\}$ and $\{\hat{x}_{laser}, \hat{y}_{laser}\}$, respectively, are parallel. The main purpose of introducing the uvz coordinate system is to make it simple to transform quantities in \mathbf{O}_{point} to that in \mathbf{O}_{laser} , or the other way around. The relationships between \mathbf{O}_{laser} , \mathbf{O}_{point} , and $\mathbf{O}_{scanner}$ are

$$\mathbf{O}_{laser} \xrightarrow{uvz} \mathbf{O}_{point} \xrightarrow{\mathbf{R}_{point}^{scanner}} \mathbf{O}_{scanner}$$

where \mathbf{R}_b^a is the relative rotation matrix from b to a , e.g. $\mathbf{R}_{point}^{scanner} = (\hat{e}_0 \hat{e}_1 \hat{e}_2)$.

3 POSITION UNCERTAINTY

A laser scanner is a kind of lidar system and can be classified as either a monostatic or a bistatic system according

to the locations of the transmitter, i.e. laser, and the receiver. A monostatic lidar is a system in which its transmitter and detector are in the almost same location. It can be divided into two different classes of systems: co-axial and bi-axial. A near-monostatic lidar is defined as a system which is close to a monostatic system and the assumption of $\mathbf{r}_{laser} \simeq \mathbf{r}_{scanner}$ is valid. Let $\text{diag}(\cdot)$ represents a diagonal matrix. In near-monostatic laser scanners, the position uncertainty of laser scanner measurement in the \mathbf{O}_{laser} coordinate system can be expressed as follow

$$\mathbf{V}(\mathbf{r})_{laser} \simeq \text{diag}(r^2 \sigma_a^2, r^2 \sigma_a^2, \sigma_r^2) \quad (3)$$

where σ_a^2 and σ_r^2 are the angular and radial uncertainties of the laser, respectively, their units are the square of radian and the square of the unit of distance, respectively, and r is the radial distance of a point from a scanner. Let us briefly look at the assumptions needed to use Eq. 3 as the variance matrix of the position uncertainty of measurement by a laser scanner. Most lidar systems are monostatic unless the problem of near-field backscattered signals by objects, i.e. aerosol, water vapour, or wall of a building close to the scanner is to be avoided. Except for a few close-range scanners, many laser scanners are monostatic or at least near-monostatic, in which we can use Eq. 3 to describe the position uncertainty of measurement. The size of transmitting region depends on the divergence angle of the laser beam and that of receiving region is decided by the size and optics of a detector. In practice, the receiving region is generally larger than transmitting region so it is reasonable to use the divergence angle of receiving region as σ_a . In addition, angular uncertainty of a laser scanner is proportional to the ratio between the divergence angles of transmitting and receiving parts (Blais et al., 2000). The radial uncertainty is how well the system can detect returning signal so it may be a function of higher order of r but we assume it is a constant. The receiving region of a laser scanner is assumed as a circle whose radii are $r\sigma_a$. From Eq. 2 and the fact that $\mathbf{V}(\mathbf{r})_{laser}$ assumes to be symmetric in the directions of \hat{x}_{laser} and \hat{y}_{laser} , i.e. Eq. 3, we can find the relationship between the position uncertainty matrices in the uvz coordinate system and \mathbf{O}_{laser} as follows

$$\mathbf{V}(\mathbf{r})_{uvz} = \mathbf{V}(\mathbf{r})_{laser}.$$

We would like to express $\mathbf{V}(\mathbf{r})_{laser}$ in \mathbf{O}_{point} . Let $\hat{e}_{i=0..2}$ be the orthonormal basis of \mathbf{O}_{point} . Then $\mathbf{V}(\mathbf{r})_{point}$ can be expressed as follows

$$\begin{aligned}\mathbf{V}(\mathbf{r})_{point} &= \mathbf{R}_{uvz}^{point} \mathbf{R}_{laser}^{uvz} \mathbf{V}(\mathbf{r})_{laser} (\mathbf{R}_{uvz}^{point} \mathbf{R}_{laser}^{uvz})^T \\ &= \mathbf{R}_{uvz}^{point} \left[\mathbf{R}_{laser}^{uvz} \mathbf{V}(\mathbf{r})_{laser} (\mathbf{R}_{laser}^{uvz})^T \right] (\mathbf{R}_{uvz}^{point})^T \\ &= \mathbf{R}_{uvz}^{point} \mathbf{V}(\mathbf{r})_{uvz} (\mathbf{R}_{uvz}^{point})^T\end{aligned}\quad (4)$$

with assumption that the variances of $\hat{e}_{i=0..2}^{uvz}$ are small. Note that $\mathbf{R}_{uvz}^{point} \simeq (\hat{e}_0^{uvz} \hat{e}_1^{uvz} \hat{e}_2^{uvz})$ where \hat{e}_i^{uvz} is the transformed vector \hat{e}_i to the uvz coordinate system. Now take into account the variance of \hat{e}_0^{uvz} and let $V(r)_{point}^{ij}$ be the i th and j th column and row of $\mathbf{V}(\mathbf{r})_{point}$. Bearing in mind that $\mathbf{V}(\mathbf{r})_{laser} = \mathbf{V}(\mathbf{r})_{uvz}$, $V(r)_{point}^{ij}$ can

be expressed as follows,

$$V(r)^{ij}_{point} \simeq (\hat{\mathbf{e}}_{i-1}^{uvz}, \mathbf{V}(\mathbf{r})_{uvz} \hat{\mathbf{e}}_{j-1}^{uvz}) + \sum_{k=\min(i,j)}^{\max(i,j)} \left(\frac{1}{2}\right)^{\delta_{ij}} (\delta_{ik} + \delta_{jk})(\mathbf{r}, \mathbf{V}(\hat{\mathbf{e}}_{k-1})\mathbf{r}) \quad (5)$$

where δ_{ij} is the Kronecker-delta symbol. In Eq. 5, the first term represents the component of $\mathbf{V}(\mathbf{r})_{laser}$ in the direction of $\hat{\mathbf{e}}_i$ and the second does the affect of the variance of $\hat{\mathbf{e}}_i$. If the variance of the estimated vector is zero, so is the second term of Eq. 5. This term is expected to be smaller than the first term if the geometric curvature is not large, i.e. for points in a flat region. In cases of higher curvature, a much larger variance of the estimated $\hat{\mathbf{e}}_i$ is expected. The approximate diagonal terms of $\mathbf{V}(\mathbf{r})_{point}$ using the uvz coordinate system, with ignorance of the second term of Eq. 5, can be expressed as follows

$$V(r)^{ii}_{point} \simeq (\hat{\mathbf{e}}_0^{uvz}, \mathbf{V}(\mathbf{r})_{uvz} \hat{\mathbf{e}}_0^{uvz}) = \cos^2 \theta_i \sigma_r^2 + \sin^2 \theta_i r^2 \sigma_a^2$$

where $\theta_{i=0..2} = \{\theta, \alpha, \beta\}$. One can find that $V(r)^{11}_{point}$ is the final result of Tasdizen and Whitaker (2003), which is the Cramer-Rao lower bound for a measurement using one laser scanner, after fixing some minor errors in their calculation since they found $\cos \theta \sigma_r^2 + \sin \theta r^2 \sigma_a^2$ as $V(r)^{11}_{point}$. The mathematical forms of the diagonal components of $\mathbf{V}(\mathbf{r})_{point}$ are the same as we expected since $\theta, \alpha,$ and β are the incidence angles of the laser beam to the surfaces whose normal vectors are $\hat{\mathbf{e}}_{i=0..2}$.

3.1 Variance of the estimated surface normal vector

In this section, we drive the variance of the estimated surface normal vector by which we can completely express the position uncertainty shown in Eq. 5. Let $\mathbf{V}(\hat{\mathbf{e}}_i)_{point}$ and $\mathbf{V}(\mathbf{r})_{point}$ be $\mathbf{V}(\hat{\mathbf{e}}_i)$ and $\mathbf{V}(\mathbf{r})$, respectively. Consider a point and its neighbourhood which are unorganised and distributed within a two dimensional elliptical region whose semi-major axes are $\hat{\mathbf{e}}_0$ and $\hat{\mathbf{e}}_1$. The component of the variance matrix of the point, $\mathbf{V}(\mathbf{r}_m)$, can be expressed as

$$\mathbf{V}(\mathbf{r}_m) = \mathbf{r}_m \mathbf{r}_m^T$$

where $\mathbf{r}_m = \mathbf{r} - \mathbf{r}_{centroid}$ and $\mathbf{V}(\mathbf{r}_m) \in \mathfrak{R}^{2 \times 2}$ in two-dimensional cases. We would like to evaluate the variance of $\hat{\mathbf{e}}_0$ and let $\sigma_{t_m}^2$ and $\sigma_{n_m}^2$ be the variances of $\hat{\mathbf{e}}_0$ in the directions of $\hat{\mathbf{e}}_1$ and $\hat{\mathbf{e}}_0$, respectively. Then they can be expressed as follows

$$\sigma_{t_m}^2 \simeq (\hat{\mathbf{e}}_1, \mathbf{r}_m \mathbf{r}_m^T \hat{\mathbf{e}}_1) = (\hat{\mathbf{e}}_1, [\mathbf{P}_{\hat{\mathbf{e}}_0} \mathbf{r}_m] [\mathbf{P}_{\hat{\mathbf{e}}_0} \mathbf{r}_m]^T \hat{\mathbf{e}}_1) \\ \sigma_{n_m}^2 \simeq (\hat{\mathbf{e}}_0, \mathbf{r}_m \mathbf{r}_m^T \hat{\mathbf{e}}_0)$$

where $\mathbf{P}_{\hat{\mathbf{e}}_i} = \mathbf{I} - \hat{\mathbf{e}}_i \hat{\mathbf{e}}_i^T$ is the projection operator of $\hat{\mathbf{e}}_i$, $\mathbf{r}_m = \mathbf{r} - \mathbf{r}_{centroid}$, and $\mathbf{P}_{\hat{\mathbf{e}}_0} \hat{\mathbf{e}}_1 = \mathbf{P}_{\hat{\mathbf{e}}_0}^T \hat{\mathbf{e}}_1 = \hat{\mathbf{e}}_1$. Note that the variance of $\hat{\mathbf{e}}_0$, $V(\hat{\mathbf{e}}_0)$, is a scalar since we are dealing with a two-dimensional case. The Cramer-Rao lower

bound for $V(\hat{\mathbf{e}}_0)$ is expressed as

$$V(\hat{\mathbf{e}}_0) = \frac{1}{\sum_{m=1}^k \frac{1}{V(\hat{\mathbf{e}}_0^m)}} \quad (6)$$

where $\hat{\mathbf{e}}_0^m$ is the estimated normal vector using only a point (Kay (1993, Ch. 3); Kanatani (1996, Ch. 3)). If we obtain an unbiased scalar estimator of a least-square problem, then Eq. 6 is the lower bound for the variance of the estimator. Bearing in mind that the variance of $\hat{\mathbf{e}}_0^m$ is inversely proportional to $\sigma_{t_m}^2$, it can be estimated as follows

$$V(\hat{\mathbf{e}}_0^m) \simeq \frac{\sigma_{n_m}^2}{\sigma_{t_m}^2},$$

therefore

$$V(\hat{\mathbf{e}}_0) \simeq \left[\sum_{m=1}^k \frac{(\hat{\mathbf{e}}_1, [\mathbf{P}_{\hat{\mathbf{e}}_0} \mathbf{r}_m] [\mathbf{P}_{\hat{\mathbf{e}}_0} \mathbf{r}_m]^T \hat{\mathbf{e}}_1)}{(\hat{\mathbf{e}}_0, \mathbf{r}_m \mathbf{r}_m^T \hat{\mathbf{e}}_0)} \right]^{-1}.$$

In general, the variance matrix of an estimated vector can be written as

$$\mathbf{V}(\hat{\mathbf{e}}_i) = \left(\sum_{m=1}^k \frac{(\mathbf{P}_{\hat{\mathbf{e}}_i} \mathbf{r}_m)(\mathbf{P}_{\hat{\mathbf{e}}_i} \mathbf{r}_m)^T}{(\hat{\mathbf{e}}_i, \mathbf{V}(\mathbf{r}_m) \hat{\mathbf{e}}_i)} \right)^{-} \quad (7)$$

where \mathbf{A}^- is the Moore-Penrose generalised inverse of a matrix \mathbf{A} (Kanatani, 1996, Ch. 7). Let $\hat{\mathbf{n}}$ be $\hat{\mathbf{e}}_0$ and it is the estimated surface normal vector of a point and its neighbourhood. Then the variance of $\hat{\mathbf{n}}$ can be decomposed into \mathbf{n}_+ and \mathbf{n}_- , which can be expressed as follows

$$\mathbf{n}_{\pm} = \hat{\mathbf{n}} \pm \sum_{i=1}^2 \mathbf{n}^i$$

where $\mathbf{n}^{i=1..2} = \sqrt{(\hat{\mathbf{e}}_i, \mathbf{V}(\hat{\mathbf{n}}) \hat{\mathbf{e}}_i)} \hat{\mathbf{e}}_i$. The variance angles of the estimated surface normal vector, $\Psi^{i=1..2}$, can be evaluated

$$\tan^2 \Psi^i = (\hat{\mathbf{e}}_i, \mathbf{V}(\hat{\mathbf{n}}) \hat{\mathbf{e}}_i) \quad (8)$$

using $\cos^2 \Psi^i = [1 + \tan^2 \Psi^i]^{-1}$ where $i = 1..2$. In the three dimensional case, we have two variance angles and if they are the same, then the variance region of the estimated normal vector is a circular cone. Otherwise, it is an elliptical cone. Now let us try to derive more explicit form of Eq. 7. With the assumptions that $\mathbf{V}(\mathbf{r}_m)$ is uniform over the neighbourhood and the change of the true normal vector within the neighbourhood of a query point is small, then

$$\sum_{m=1}^k \frac{(\mathbf{P}_{\hat{\mathbf{n}}} \mathbf{r}_m)(\mathbf{P}_{\hat{\mathbf{n}}} \mathbf{r}_m)^T}{(\hat{\mathbf{n}}, \mathbf{V}(\mathbf{r}_m) \hat{\mathbf{n}})} = \sum_{m=1}^k \frac{(\mathbf{P}_{\hat{\mathbf{n}}} \mathbf{r}_m)(\mathbf{r}_m^T \mathbf{P}_{\hat{\mathbf{n}}})}{(\hat{\mathbf{n}}, \mathbf{V}(\mathbf{r}_m) \hat{\mathbf{n}})} \\ \simeq \frac{k}{(\hat{\mathbf{n}}, \mathbf{V}(\mathbf{r}_m^{query}) \hat{\mathbf{n}})} \left[\sum_{i=1}^2 \lambda_i \hat{\mathbf{e}}_i \hat{\mathbf{e}}_i^T \right] \quad (9)$$

since $\mathbf{P}_{\hat{\mathbf{n}}} \hat{\mathbf{n}} = \mathbf{0}$, where $\mathbf{r}_m^{query} = \mathbf{r}^{query} - \mathbf{r}_{centroid}$. The rank of Eq. 9 is two in cases of three-dimensional point

clouds and its Moore-Penrose generalised inverse is the variance of the estimated normal vector that is given as follows

$$\begin{aligned} \mathbf{V}(\hat{\mathbf{n}}) &= \left\{ \frac{k}{(\hat{\mathbf{n}}, \mathbf{V}(\mathbf{r}_m^{query})\hat{\mathbf{n}})} \left[\sum_{i=1}^2 \lambda_i \hat{\mathbf{e}}_i \hat{\mathbf{e}}_i^T \right] \right\}^{-} \\ &= \frac{(\hat{\mathbf{n}}, \mathbf{V}(\mathbf{r}_m^{query})\hat{\mathbf{n}})}{k} \left[\sum_{i=1}^2 \frac{1}{\lambda_i} \hat{\mathbf{e}}_i \hat{\mathbf{e}}_i^T \right]. \end{aligned} \quad (10)$$

Note that we have evaluated the variance matrix of the eigenvectors in \mathbf{O}_{point} using $\mathbf{r}_m = \mathbf{r} - \mathbf{r}_{centroid}$. Then the diagonal component of $\mathbf{V}(\mathbf{r})_{point}$ can be expressed as follows

$$\begin{aligned} V(\mathbf{r})_{point}^{(i,j)} &= (\hat{\mathbf{e}}_{i-1}^{uvz}, \mathbf{V}(\mathbf{r})_{uvz} \hat{\mathbf{e}}_{j-1}^{uvz}) \\ &+ \sum_{k=\min(i,j)}^{\max(i,j)} 2 \left(\frac{1}{2} \right)^{\delta_{ij}} (\delta_{ik} + \delta_{jk}) (\mathbf{r}_m, \mathbf{V}(\hat{\mathbf{e}}_k) \mathbf{r}_m) \\ &= (\hat{\mathbf{e}}_{i-1}, \mathbf{V}(\mathbf{r}) \hat{\mathbf{e}}_{j-1}) \\ &+ \sum_{k=\min(i,j)}^{\max(i,j)} 2 \left(\frac{1}{2} \right)^{\delta_{ij}} (\delta_{ik} + \delta_{jk}) (\mathbf{r}_m, \mathbf{V}(\hat{\mathbf{e}}_k) \mathbf{r}_m) \end{aligned} \quad (11)$$

since $(\hat{\mathbf{e}}_{i-1}, \mathbf{V}(\mathbf{r}) \hat{\mathbf{e}}_{j-1}) = (\hat{\mathbf{e}}_{i-1}^{uvz}, \mathbf{V}(\mathbf{r})_{uvz} \hat{\mathbf{e}}_{j-1}^{uvz})$ and $\mathbf{V}(\mathbf{r})_{laser} = \mathbf{V}(\mathbf{r})_{uvz}$. Note that the only reason for the revision of Eq. 5 into Eq. 11 is that we have calculated the variance of the normal vector using \mathbf{r}_m^{query} . With the assumption that $\frac{\mathbf{r}}{|\mathbf{r}|} \simeq \hat{\mathbf{z}} \simeq \frac{\mathbf{r}_{centroid}}{|\mathbf{r}_{centroid}|}$, $\mathbf{V}(\mathbf{r}) \simeq \mathbf{V}(\mathbf{r}_{centroid})$, $\mathbf{V}(\mathbf{r}_m) \simeq \frac{1}{2} \mathbf{V}(\mathbf{r})$, and $\mathbf{V}(\mathbf{r}_m^{query}) \simeq \frac{1}{2} \mathbf{V}(\mathbf{r}^{query})$, the component of $\mathbf{V}(\hat{\mathbf{n}})$ in the direction of $\frac{\mathbf{r}_m}{|\mathbf{r}_m|}$ can be approximately expressed as follows

$$\begin{aligned} (\mathbf{r}_m, \mathbf{V}(\hat{\mathbf{n}}) \mathbf{r}_m) &\simeq r^2 (\hat{\mathbf{z}}, \mathbf{V}(\hat{\mathbf{n}}) \hat{\mathbf{z}}) - r_{centroid}^2 (\hat{\mathbf{z}}, \mathbf{V}(\hat{\mathbf{n}}) \hat{\mathbf{z}}) \\ &= (r^2 - r_{centroid}^2) \\ &\times \frac{(\hat{\mathbf{n}}, \mathbf{V}(\mathbf{r}_m^{query})\hat{\mathbf{n}})}{k} \left(\hat{\mathbf{z}}, \left[\sum_{i=1}^2 \frac{1}{\lambda_i} \hat{\mathbf{e}}_i \hat{\mathbf{e}}_i^T \right] \hat{\mathbf{z}} \right) \\ &= \frac{1}{2} (r^2 - r_{centroid}^2) \frac{(\hat{\mathbf{n}}, \mathbf{V}(\mathbf{r}^{query})\hat{\mathbf{n}})}{k} \\ &\times \left[\frac{1}{\lambda_1} \cos^2 \alpha + \frac{1}{\lambda_2} \cos^2 \beta \right]. \end{aligned} \quad (12)$$

From Eqs. 11 and 12, we have a complete and explicit form of $\mathbf{V}(\mathbf{r})_{point}$. For example, $V(\mathbf{r})_{point}^{11}$ is expressed as follow

$$\begin{aligned} V(\mathbf{r})_{point}^{11} &\simeq (\hat{\mathbf{e}}_0, \mathbf{V}(\mathbf{r}^{query})\hat{\mathbf{e}}_0) + (\mathbf{r}, \mathbf{V}(\hat{\mathbf{e}}_0) \mathbf{r}) \\ &= \cos^2 \theta \sigma_r^2 + \sin^2 \theta r^2 \sigma_a^2 \\ &+ (r^2 - r_{centroid}^2) \frac{(\hat{\mathbf{e}}_0, \mathbf{V}(\mathbf{r}^{query})\hat{\mathbf{e}}_0)}{k} \\ &\times \left[\frac{1}{\lambda_1} \cos^2 \alpha + \frac{1}{\lambda_2} \cos^2 \beta \right]. \end{aligned}$$

The second term of Eq. 11 is expected to be small since they are propositional to the differences between the squared radial distances of the query point and the centroid of its neighbourhood, i.e. $(r^2 - r_{centroid}^2)$. The color

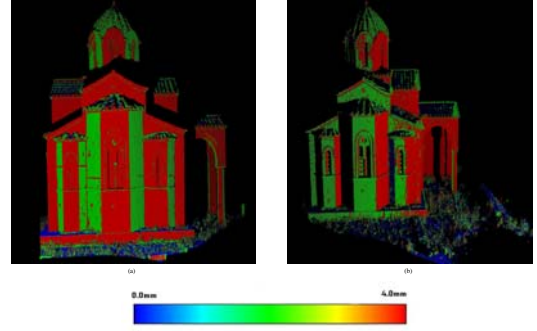


Figure 3: (a) and (b) are $\sqrt{(\hat{\mathbf{n}}, \mathbf{V}(\mathbf{r}))\hat{\mathbf{n}}}$, i.e. the squared root of the first term of Eq. 11, of the Agia Sanmarina church in Greece scanned from different locations using a Leica HDS2500.

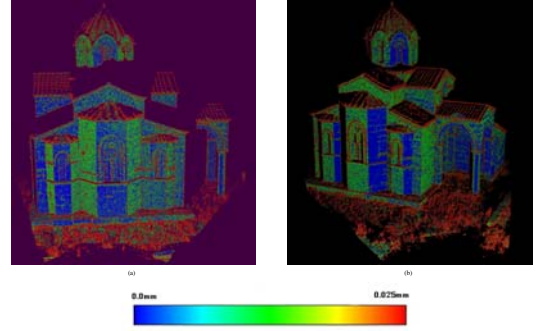


Figure 4: (a) and (b) are $\sqrt{(\hat{\mathbf{r}}, \mathbf{V}(\hat{\mathbf{n}}))\hat{\mathbf{r}}}$, i.e. the squared root of the second term of Eq. 11, of the Agia Sanmarina church in Greece scanned from different locations using a Leica HDS2500.

maps of $(\hat{\mathbf{n}}, \mathbf{V}(\mathbf{r}))\hat{\mathbf{n}}$ and $(\mathbf{r}, \mathbf{V}(\hat{\mathbf{n}})\mathbf{r})$ of two point clouds scanned from two different locations are presented in Figures 3 and 4. For the Leica HDS2500, the effect of the radial variance in the direction of the surface normal vector is about a hundred times larger than that of $(\mathbf{r}, \mathbf{V}(\hat{\mathbf{n}})\mathbf{r})$. In Figure 3, we can also observe that there is about 2mm of the difference in $\sqrt{(\hat{\mathbf{n}}, \mathbf{V}(\mathbf{r}))\hat{\mathbf{n}}}$ between the overlapping regions of the point clouds.

4 EXPERIMENTS

From the previous section, we can see that primarily two factors contribute to position uncertainty, the scanning hardware and the estimation of the surface normal direction. While there is little that can be done to reduce the errors cause by the hardware, the errors caused by variance in surface normal direction can be reduced. Expand Eq. 10 to get the form

$$\Psi^{i=1\dots 2} = \tan^{-1} \left\{ \left[\frac{\cos^2 \theta \sigma_r^2 + \sin^2 \theta r^2 \sigma_a^2}{k \lambda_i} \right]^{\frac{1}{2}} \right\} \quad (13)$$

We can see that the variance angle is effected by two variables, the number of points in the neighbourhood and the eigenvalues of the covariance matrix of the neighbourhood. The eigenvalues are affected by the number of points and their distribution within the neighbourhood in an unorganised point cloud. When the eigenvalues are plotted against

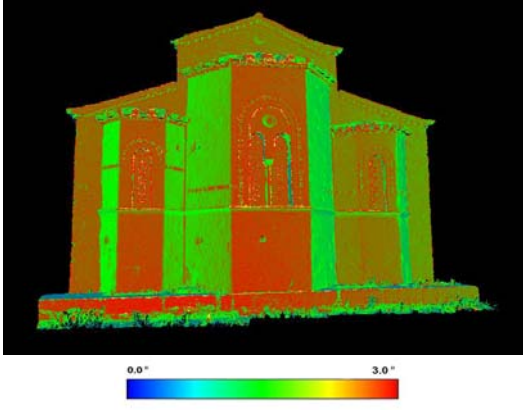


Figure 5: variance angle of the estimated surface normal with a neighbourhood size of 30.

the number of neighbourhood points, we can clearly see a linear relationship, as shown in Figure 6.

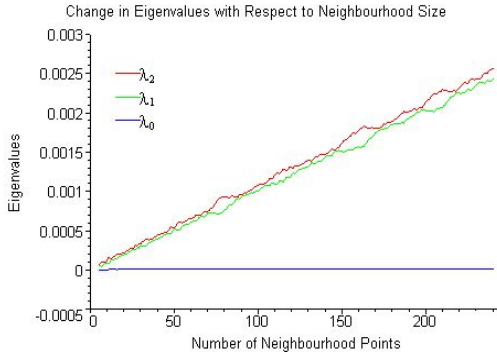


Figure 6: Eigenvalues plotted against the number of points in the neighbourhood where $\lambda_0 \leq \lambda_1 \leq \lambda_2$. Note that if $k = 0$, then there is only one datum, i.e. the query point.

If we let $\lambda_i = \kappa k + \tau$ for some constants κ and τ which can be numerically estimated for a point cloud, then Eq. 13 becomes

$$\Psi^{i=1..2} = \tan^{-1} \left\{ \left[\frac{\cos^2 \theta \sigma_r^2 + \sin^2 \theta r^2 \sigma_a^2}{\kappa k^2 + \tau k} \right]^{\frac{1}{2}} \right\} \quad (14)$$

meaning the variance angle becomes a function of order $\Theta\left(\frac{1}{k^2}\right)$. This can be seen if we plot the average variance angle of a point cloud against the neighbourhood size, as in Figure 7.

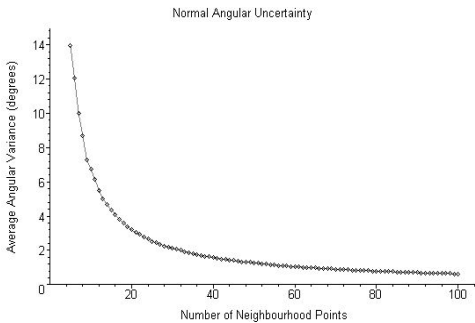


Figure 7: Average variance angle in the normal vector

We can also use this information to find the local neighbourhood size. Mitra et al. (2004) have proposed a method of finding a radius for each neighbourhood given a threshold value, with an improvement to the method discussed by Lalonde et al. (2005). While they focused on the radius of the neighbourhood, we will focus on finding the number of points in a neighbourhood based on a given threshold for the variance angle. The obvious method to find the neighbourhood number is to iteratively increase the number by one until the variance angle of the normal is less than the specified tolerance (a time consuming and computationally expensive process). While the local neighbourhood size will differ, it will still follow the trend shown for the global attribute as presented in Figure 7. Therefore, an easy way to speed up the iterative procedure is to only look a neighbourhood size of 2^k since as k increases, larger step sizes will need to be taken to produce any significant changes. A better way to find the local neighbourhood size is if Eq. 10 is reformatted to produce an approximate value in one step. Assuming that an approximate normal direction $\hat{\mathbf{n}}_{init}$ was found with an initial neighbourhood size of k_{init} and we are given a tolerance of Ψ_{tol} for the angular variance of the normal, we can determine an approximate value for k as follows

$$k_i \lambda_i = \frac{(\hat{\mathbf{n}}_{init}, \mathbf{V}(\mathbf{r}_{query}) \hat{\mathbf{n}}_{init})}{\tan^2(\Psi_{tol})} \quad (15)$$

where $i = 1..2$. We also need to determine what value λ_i will take on for k . We know that it has a linear relationship with respect to k as shown in Figure 6. If we assume that τ is zero, then we can approximate Eq. 15 with,

$$\lambda_i(k) = \frac{\lambda_i(k_{init})}{k_{init}} k_i$$

where $\lambda_i(k)$ is the eigenvalue for the neighbourhood size of k in i th iteration. Substitute this into Eq. 15, we obtain,

$$k_i = \left[\frac{k_{init} (\hat{\mathbf{n}}_{init}, \mathbf{V}(\mathbf{r}_{query}) \hat{\mathbf{n}}_{init})}{\tan^2 \Psi_{tol} \lambda_i(k_{init})} \right]^{\frac{1}{2}} \quad (16)$$

and we use the maximum of k_i as k .

Procedure 1 Estimate Local Neighbourhood Size

Require: κ for Eq. 14 is estimated and τ is assume to be zero.

- 1: $k_{new} \leftarrow k_{init}$
 - 2: Evaluate $\hat{\mathbf{n}}(k_{new})$, $\lambda_1(k_{new})$, and $\lambda_2(k_{new})$
 - 3: **while** $\Psi_{new} < tolerance$ **do**
 - 4: **if** $k_{new} \leq k$ {If it doesn't converge.} **then**
 - 5: $k_{new} \leftarrow k_{init} + 2^{iteration}$
 - 6: Evaluate $\hat{\mathbf{n}}(k_{new})$, $\lambda_1(k_{new})$, and $\lambda_2(k_{new})$
 - 7: **end if**
 - 8: $k \leftarrow k_{new}$
 - 9: $k_{new} \leftarrow Eq. ??$
 - 10: Update $\hat{\mathbf{n}}(k_{new})$, $\lambda_1(k_{new})$, and $\lambda_2(k_{new})$
 - 11: $\Psi_{new} \leftarrow \max(Eq. 14)$
 - 12: **end while**
 - 13: **return**(k_{new})
-

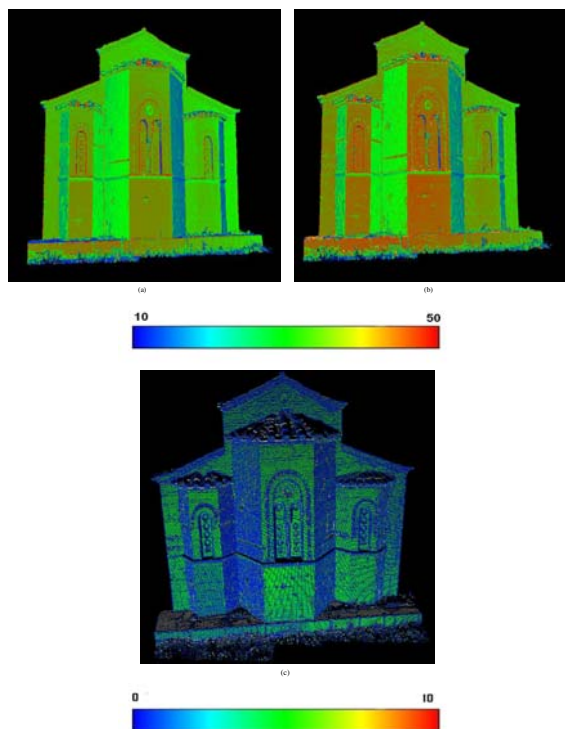


Figure 8: (a) shows the exact local neighbourhood number while (b) shows the approximated value using the proposed algorithm which minimise the variance angles of points in terms of the global and local. (c) shows the difference in the variance angles and the white represents that its difference in the variance angle is greater than 10.

Since the shape of the variance angle curve is a function of k and λ_i , unless the estimation of the surface normal vectors is good and the linear relationship between k and λ_i is strong, then the approximate value for k (for a given threshold value of the angular variance) will be under or over estimated. This problem can be reduced by recalculating the surface normal and eigenvalues as well as the relationship between λ_i and k . This problem may persist if the threshold value is relatively smaller than the true variance since the slight difference in the true and estimated variance curves (from incorrect λ_i approximation) will result in large difference in k . The algorithm is briefly described in Procedure. 4.

Applying the algorithm to the church dataset, we see the results presented in Figure 8. Using a tolerance of 2° on the variance angle of the surface normal, an average of 1.26 iterations were performed after finding an approximate value of the normal and eigenvalues using an initial neighbourhood size of 10. As shown in Figure 8, most of the approximate values of k are close to the true values found through iteration, although some values are overestimated. The mean and standard deviation of the difference in the sizes of neighbourhood are 2.93 and 0.007, respectively. The mean of the difference in the sizes of neighbourhood is about 1% of the mean neighbourhood size using the exact method. At this tolerance, there were no problems with convergence. In the regions where the density of points is low, we can find larger difference between the exact and approximate methods.

5 CONCLUSION

An explicit form of position uncertainty in unorganised point clouds from laser scanners was presented by means of the covariance analysis of a point. We also derived an explicit form of the variance of the estimated surface normal vector of a point. Both are important and must be taken into account in any estimation within a point cloud from laser scanners.

The properties of the global optimal size of the neighbourhood were investigated. In addition, an algorithm to iteratively evaluate a local optimal size of the neighbourhood of a point which minimises the variance of the estimated normal vector of the point was developed.

6 ACKNOWLEDGEMENT

We would like to thank to Stuart Gordon, Mike Stewart, and Maria Tsakiri for the provision of the Agia Samarina church dataset. The work has been in parts supported by the Australian Research Council, Curtin University of Technology and the Cooperative Research Centre for Spatial Information, whose activities are funded by the Australian Commonwealth's Cooperative Research Centres Programme.

References

- Bae, K.-H. and Lichti, D. D., 2004. Automated registration of unorganised point clouds from terrestrial laser scanners. *International Archives of Photogrammetry and Remote Sensing (IAPRS) 35(part B5)*, pp. 222–227.
- Blais, F., Beraldin, J. A. and El-Hakim, S., 2000. Range error analysis of an integrated time-of-flight, triangulation, and photogrammetric 3D laser scanning system. *Proceedings of SPIE's Aerosense*.
- Kanatani, K., 1996. *Statistical optimization for geometric computation: theory and practice*. first edn, Elsevier Science.
- Kay, S. M., 1993. *Fundamentals of Statistical Signal Processing : Estimation Theory*. first edn, Prentice Hall.
- Lalonde, J.-F., Unnikrishnan, R., Vandapel, N. and Hebert, M., 2005. Scale selection for classification of point-sampled 3-D surfaces. Technical Report CMU-RI-TR-05-01, Robotics Institute, Carnegie Mellon University, Pittsburgh, PA.
- Mitra, M. J., Nguyen, A. and Guibas, L., 2004. Estimating surface normals in noisy point cloud data. *International Journal of Computational Geometry and Applications* 14(4,5), pp. 261–276.
- Tasdizen, T. and Whitaker, R., 2003. Cramer-Rao bounds for nonparametric surface reconstruction from range data. *Proceedings of 3-D Digital Imaging and Modelling (3DIM)*.